New Calculational Method for Epitaxial Energy: Application to an Axial Commensurate Interface

Sun M. Paik and Ivan K. Schuller
Physics Department, B-019, University of California, San Diego, La Jolla, California 92093
(Received 5 July 1989)

A new "mapping technique" is introduced which allows the study of epitaxy in systems that are commensurate or incommensurate. This method is applied to the epitaxy of fcc(111)/bcc(110) which is commensurate in one direction and incommensurate in the other. The mapping technique predicts a new epitaxial orientation, in good agreement with recent experimental results. The use of second-order perturbation theory in conjunction with the mapping technique predicts a change in epitaxial orientations as a function of island size and stiffness of overlayer lattice.

PACS numbers: 68.55.Gi, 68.55.Jk

A microscopic understanding of the nature of epitaxy has been a long-standing subject of experimental[1-3] and theoretical[4-8] interest. Recent developments and capabilities, in experimental techniques and computational methods, have given a renewed impetus to studies geared towards the understanding of epitaxial growth at the microscopic level. Epitaxial growth has been experimentally accomplished in a large number of systems including lattice-matched and -mismatched systems. Theoretical efforts have been based on a number of phenomenological methods,[4-6] Monte Carlo simulations,[7] and molecular-dynamics simulations.[8] However, in many cases, these methods are not able to predict satisfactorily the energetics of epitaxial growth, especially as a function of system size and temperature. We present here a novel computational method ("*mapping technique*") which allows the calculation of epitaxial energies in large-sized commensurate and incommensurate systems. This technique is then applied to the extensively studied fcc(111)/bcc(110) system, which is only commensurate along one crystallographic direction. We find a new epitaxial orientation, so far unpredicted, which is in good agreement with experimental observation.[9] The mapping technique in conjunction with second-order perturbation theory predicts a change in epitaxial orientation as a function of size and stiffness of lattices in qualitative agreement with a molecular-dynamics simulation.

An ideal epitaxial configuration (IEC) is obtained when two lattices which may differ in symmetry are in a coherent lattice-matching situation,[4] i.e., for instance, in one-dimensional interfaces, when the lattice-constant ratio $\rho = b_a/b_s$ is a rational number, where b_a and b_s are surface lattice constants of overlayer (a) and substrate (s) lattices, respectively (for two-dimensional interfaces, it also depends on the relative orientation θ). There are an infinite number of the coherent matches. However, considering the interfacial energy difference between the coherent and noncoherent matches, most coherent matches are indistinguishable from noncoherent matches in an experiment, except for very few coherent matches [for example, only four matches in the fcc(111)/bcc(110) system, as will be seen later]. Only these few coherent matches will be labeled as IEC and we define the lattice-constant ratio of this system as ρ_c. For configurations away from the ideal, ρ_N ($\neq \rho_c$), the total adatom-substrate (a-s) interaction energy (V_{as}) forces all adatoms to be matched coherently with the substrate lattice whereas the total adatom-adatom (a-a) interaction energy (V_{aa}) tends to keep adatoms in the equilibrium positions of the natural (unstrained) overlayer structure. The system reaches equilibrium at an intermediate configuration ρ', between ρ_N and ρ_c, at which the driving force toward an IEC by the total a-s interaction $[-(\Delta V_{as}/\Delta\rho)|_{\rho'}]$ is equal in magnitude and opposite in direction to the strain force $[-(\Delta V_{aa}/\Delta\rho)|_{\rho'}]$. However, for an infinite-size system at zero temperature, the total a-s interaction exhibits δ-function-like minima as a function of the lattice-constant ratio ρ at the exact commensurate lattice points, i.e., $V_{as}(\rho) = \sum_{\rho_c} V_0(\rho_c) \times \delta(\rho_c - \rho)/\delta_0$, where $\delta(0)/\delta_0 = 1$. Thus, for infinitely large non-IEC systems, a strained epitaxial layer cannot be formed since the driving force, $-\Delta V_{as}/\Delta\rho$, is zero. In real systems, however, these δ-function minima are broadened due to finite-size and finite-temperature lattice relaxations. Although understanding these broadening effects is very important for epitaxial growth, to our knowledge no clear-cut theoretical scheme has emerged which allows systematic studies of the finite size and temperature dependence of epitaxy.

In this Letter, we introduce a new technique (*mapping technique*) to study epitaxy which addresses the issues raised above. The two assumptions of this technique are as follows: (1) The original crystal symmetry of the two lattices is undisturbed by the a-s interactions; (2) the a-s interaction potential has the periodicity and symmetry of the substrate surface lattice. Clearly, the first assumption is a rather oversimplified situation for a real system. The rigidity criterion has been tested from the misfit dislocation analysis.[5] In fact, many metal-on-metal systems exist for which the rigid model (and the elastic model) provides an adequate description.[5] The calculation is done in two steps. First, we calculate the ideal epitaxial configurations and broadening of energy minima due to finite-size effects using the mapping technique. Then, we calculate temperature effects using second-order perturbation theory and

© 1990 The American Physical Society

compare with the usual molecular-dynamics-simulation results. As an example, we study the fcc(111)/bcc(110) system. However, our methodology can readily be extended to any lattice-mismatched system.

Because the a-s interaction is assumed to have the periodicity and symmetry of the substrate surface lattice, the total a-s interaction per adatom can be written as

$$V_{as}=\frac{1}{N_a}\sum_i^{N_a}\sum_j^{N_s}V(\mathbf{r}_i,\mathbf{r}_j)=\frac{1}{N_a}\sum_{\mathbf{G}}V_{\mathbf{G}}\sum_i^{N_a}e^{-i\mathbf{G}\cdot\mathbf{r}_i}, \quad (1)$$

where $\mathbf{G}$ are reciprocal-lattice vectors, $\mathbf{r}_i$ denotes the position of adatoms, and N_a, N_s are the total number of overlayer and substrate atoms, respectively. Since the potential, Eq. (1), is a one-particle potential and periodic with the substrate-surface-lattice vectors, a convenient way to evaluate Eq. (1) is to map all the overlayer atoms into a unit cell of the substrate lattice. For a large system, the summation over i in Eq. (1) can be converted to an integration over the unit cell:

$$V_{as}=\sum_{\mathbf{G}}V_{\mathbf{G}}\frac{1}{v_c}\int_{\text{cell}}d\mathbf{r}f(\mathbf{r})e^{-i\mathbf{G}\cdot\mathbf{r}}e^{-i\mathbf{G}\cdot\mathbf{r}_0}, \quad (2)$$

where "*cell*" denotes integration over the substrate-surface-lattice unit cell, v_c is volume of a unit cell, $f(\mathbf{r})$ is a distribution function, and $\mathbf{r}_0$ is the origin of the overlayer. For the lattice-constant ratio $\rho=n/m$,[10] where n and m are integers (denoted as "mth-order" commensurate lattices), $f(\mathbf{r})$ will be m equally spaced points in the unit cell. The leading-order term in V_{as}, of mth-order commensurate lattice, is proportional to the mth-order term in the Fourier series of the overlayer-substrate potential. When $m=1$, the mapping pattern, $f(\mathbf{r})$, is a single point and V_{as} is lowest.

For incommensurate lattices, $f(\mathbf{r})$ will be a uniform, constant distribution. V_{as} of the incommensurate lattice is just the space average of the potential, $V_{\mathbf{G}=0}=(1/v_c)\times\int_{\text{cell}}d\mathbf{r}\,V(\mathbf{r})$. For a short-range interaction, V_{as} for a high-order commensurate lattice ($m>3$) is very small, since the corresponding terms in the Fourier series are small and almost the same as those of the incommensurate lattices. Thus, the commensurate-lattice matches $\rho_c=n/m$ (Ref. 10) for $m\leq 3$ will be labeled as IEC. For an infinite system, V_{as} consists of δ-function-like minima at IEC because configurations slightly away from IEC are either incommensurate or very-high-order commensurate (which is not much different from incommensurate as far as energy is concerned). For a finite-size system, however, the distribution $f(\mathbf{r})$ is not uniform and may be concentrated in selected areas of the substrate unit cell, and as a consequence, the interfacial energy minimum will have a finite width.

The fcc(111)/bcc(110) system is particularly interesting since it has been extensively studied, both experimentally[3,9] and theoretically,[4,5] using conventional techniques. In this system, the two lattices can only be incommensurate or partially commensurate. (A system commensurate along the x or y direction must be incommensurate along the other direction.[11] This is denoted as an "*axial commensurate*" system.) For more than fifty years only two epitaxial orientations have been found experimentally and theoretically: Kurdjumov-Sachs (KS) orientation[12] ($\rho=1.089$, $\theta=5.26°$) and Nishiyama-Wassermann (NW) orientations[13] ($\rho=0.943$, $\theta=0°$ and $\rho=1.155$, $\theta=0°$). Recently, an experimental study[9] observed a new orientation [Homma-Yang-Schuller (HYS)] for $\rho=1.333$, $\theta=30°$.

TABLE I. Relative orientations θ, lattice-constant ratio ρ at minima, and width a of the interfacial energy minima, $V_{as}=V_{as}(\rho)$, for the first four lowest-order axial commensurate lattice-matched systems of fcc(111)/bcc(110). The fourth column represents the reciprocal-lattice vectors, $\mathbf{G}_n$, that contribute to the energy minima and $\mathcal{R}$ is the radius of a cluster disk. Once the functional form of the a-s potential is specified, the well depth can be calculated as discussed in the text.

Orientation	θ	ρ	a	$\mathbf{G}_n$
NW	0°	$\frac{2\sqrt{2}}{3}$	$\frac{3\sqrt{2}\pi\mathcal{R}}{2b_a}$	$\frac{\sqrt{3}n\pi}{b_s}(0,\sqrt{2})$
		$\frac{2}{\sqrt{3}}$	$\frac{2\sqrt{3}\pi\mathcal{R}}{b_a}$	$\frac{\sqrt{3}n\pi}{b_s}(2,0)$
KS	5.26°	$\frac{4\sqrt{2}}{3\sqrt{3}}$	$\frac{3\sqrt{3}\pi\mathcal{R}}{2\sqrt{2}b_a}$	$\frac{\sqrt{3}n\pi}{b_s}(1,1/\sqrt{2})$
HYS	30°	$\frac{4}{3}$	$\frac{3\pi\mathcal{R}}{b_a}$	$\frac{\sqrt{3}n\pi}{b_s}(2,0)$

We apply the mapping technique described in the previous paragraph to calculate the ideal epitaxial configurations. We find an infinite number of axial commensurations but only one first-order[14] ($\rho=4\sqrt{2}/3\sqrt{3}$, $\theta=\tan^{-1}[(\sqrt{6}-2)/(\sqrt{2}+2\sqrt{3})]\approx 5.26°$, KS orientation), one second-order[14] ($\rho=2\sqrt{2}/3$, $\theta=0°$, NW orientation), and two third-order[14] ($\rho=2/\sqrt{3}$, $\theta=0°$, NW orientation and $\rho=\frac{4}{3}$, $\theta=30°$, HYS orientation[9]) commensurate matches. The results for these four leading-order epitaxial orientations are reported in Table I. V_{as} for higher-order commensurate matches are too small to be observed experimentally.

Figure 1 shows the mapping pattern for a circular overlayer of $N=9961$ atoms near the KS orientation ($\rho_c=1.089$). The mapping pattern is a constant distribution along the incommensurate axis (y') and a band along the commensurate axis (x'). Considering a circular disk of radius $\mathcal{R}$ mapped into the band, the distribution function can be approximated by $f(\mathbf{r})=(4/x_0\pi)\times[1-(x'/x_0)^2]^{1/2}$ for $|x'/x_0|\leq 1$ and $f(\mathbf{r})=0$ for $|x'/x_0|>1$, where $x_0=c\mathcal{R}b_s\Delta\rho/b_a$ is the half-width of the band, c is a constant that depends on epitaxial orientation, x' is a position variable along the axial commensurate axis (see Fig. 1), and $\Delta\rho=|\rho-\rho_c|$. After integration of Eq. (2) with the above $f(\mathbf{r})$, the size-dependent V_{as} becomes

$$V_{as}=\sum_{\mathbf{G}}V_{\mathbf{G}}[J_1(a\Delta\rho)/a\Delta\rho]\delta_{\mathbf{G}_\perp=0}, \quad (3)$$

where J_1 is the Bessel function of the first kind, $\mathbf{G}=\mathbf{G}_\perp$

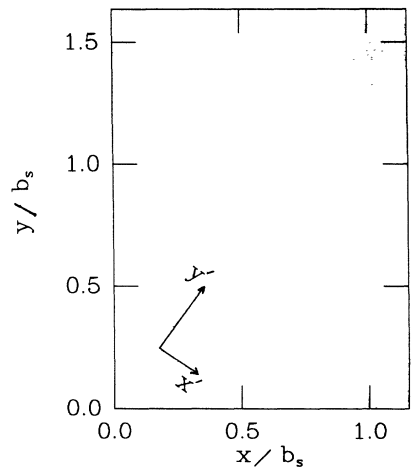

FIG. 1. The mapping pattern, $f(\mathbf{r})$, for a 9961 circular adatom cluster near KS orientation. x' and y' denote commensurate and incommensurate axes, respectively.

$+\mathbf{G}_{\parallel}$, $\mathbf{G}_{\perp}$ and $\mathbf{G}_{\parallel}$ denote the reciprocal-lattice vectors of the substrate surface lattice along the direction perpendicular and parallel to the axial commensuration, respectively, and $a=|G_{\parallel}|c\mathcal{R}b_s/b_a$ is given in Table I. The shape of the miminum depends on the geometrical shape of the cluster but does not depend much on the details of the potential as long as $V_{\mathbf{G}}$ decreases rapidly with increasing $\mathbf{G}$. The reciprocal-lattice vectors that satisfy the condition $\delta_{\mathbf{G}_{\perp}=0}$ are presented in Table I for all four epitaxial orientations. Once the functional form of the potential $V_{\mathbf{G}}$ is specified, the well depth can be calculated from Eq. (3). As the size of cluster increases $N_a \to \infty$ (i.e., $\mathcal{R} \to \infty$) the δ-function-like minimum is recovered. Further details of the calculation will be published elsewhere.[15]

In Table II, we present V_{as} for two different sizes of the overlayer at a lattice-constant ratio $\rho=1.14$. For the smaller size, $N_a=127$, the KS orientation is lower in energy than the NW orientation, whereas the NW orientation is lower for the larger one, $N_a=547$ (V_{as} does not depend on the relative orientation of the overlayer). Thus, there must be a crossover region where an epitaxial orientation shift from KS orientation to one of the NW orientation ($\rho=1.155$, $\theta=0°$) as the overlayer grows in an experiment.

In order to study finite-temperature effects, we employ a second-order perturbation calculation. For the sake of simplicity, we consider a situation wherein the substrate lattice is much stiffer than the overlayer lattice (which may be a good approximation for a case of a thin adsorbed layer). By treating the a-s interaction as a perturbation to the a-a (and s-s) interaction, second-order perturbation theory yields

$$E^{(2)} \approx -\sum_{\mathbf{K},\mathbf{G}} V_{\mathbf{G}}^2 |\mathbf{G}|^2 e^{-2W}/2M_a v_a^2 |\mathbf{K}-\mathbf{G}|^2, \quad (4)$$

where M_a, $\mathbf{K}$, $\mathbf{G}$, v_a, and e^{-2W} are mass of an adatom, reciprocal-lattice vectors of overlayer and substrate lattices, the velocity of sound on the overlayer, and the Debye-Waller factor, respectively. Since perturbation theory is not valid for small $|\mathbf{K}-\mathbf{G}|$ (hence small $\Delta\rho$), we are not able to estimate accurate temperature-dependent results especially near the minimum. However, we can investigate some qualitative feature of temperature effects and compare with numerical molecular-dynamics (MD) results. We note that a more rigorous theory is necessary for an accurate calculation of temperature effects on the interfacial energy of real system.

For comparisons at finite temperature, we employ a standard molecular-dynamics-simulation technique for a 397-atom hexagonal overlayer cluster on a 1141-atom movable-substrate layer that is supported by a rigid bcc(110) substrate layer. In order to prevent the overlayer from rotating (or orientational oscillation) during the calculation of the orientation-dependent V_{as} at an angle away from minima, a rigid fcc(111) template is used to hold the overlayer at a fixed angle. For a-s and a-a interaction potentials, the well-known Lennard-Jones (LJ) 12-6 potential with a cutoff at $r_c=2.5\sigma$ is employed and a harmonic potential is used for bcc substrate-substrate interaction potentials. Initially, adatoms are placed in the close-packed positions (a stable configuration for a LJ system) and substrate atoms at bcc(110) lattice points. The velocity of the atoms is assigned according to the Maxwell-Boltzmann distribution. The potential strength between an adatom and a substrate atom is 0.125ϵ, whereas a-a and s-s interaction potential strengths are ϵ. These potential strengths are chosen so that the *overlayer* and *substrate* keep their crystal symmetry.[5] The simulation is carried out to calculate V_{as}, at temperatures $T=0.0$ and 0.1 (bulk melting temperature of the LJ solid is $T_m=0.68$)[8] in standard LJ units in which σ, ϵ, ϵ/k_B, and $t_0=(m\sigma^2/\epsilon)^{1/2}$ are the length, energy, temperature, and time units, respectively, where m and k_B are the mass of each atom and the Boltzmann constant.

MD results are plotted in Fig. 2, at $T=0.0$ (open circles), and at $T=0.1$ (solid squares) for a KS orientation as a function of the lattice-constant ratio ρ. V_{as} calculated by the mapping technique for 397 atoms is included (solid line). In order to evaluate Eq. (4) (dotted line in Fig. 2), v_a is calculated from the dynamical matrix of the LJ crystal for the polarization vector parallel to $\mathbf{G}$ and the Debye-Waller factor is calculated from the nu-

TABLE II. Overlayer-substrate interaction energy at $\rho=1.14$ for two different overlayer cluster sizes.

Orientation	N_a	V_{as}/ϵ
NW	547	−0.077
		−0.071
KS	127	−0.080
		−0.099

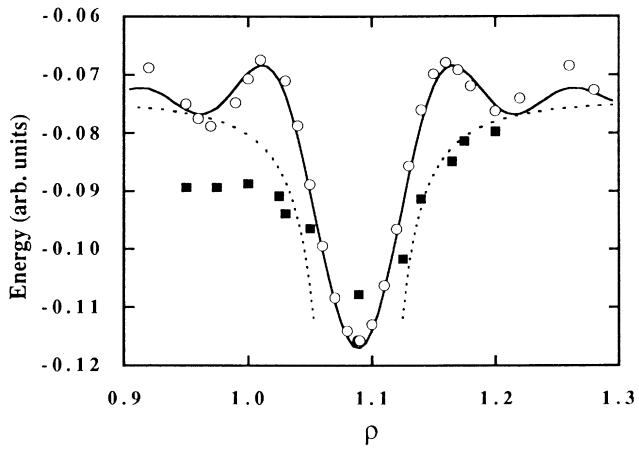

FIG. 2. Energy per overlayer particles of the fcc(111)/bcc(110) system, as a function of lattice-constant ratio near the KS orientation for a total number of adatoms $N_a=397$. The open circles and solid squares represent MD results at temperatures $T=0.0$ and 0.1 in LJ units, respectively. The solid line is the calculated results using the mapping technique at $T=0.0$ (to be compared with the open circles) and the dotted line using second-order perturbation theory at $T=0.1$ (to be compared with the solid squares).

merical results of the mean-square displacement $\langle |\mathbf{u}|^2 \rangle$. At zero temperature, our numerical results are in excellent agreement with the analytic calculation using the mapping technique. At finite temperatures, the perturbation-calculation results qualitatively agree with the MD results. The anisotropic broadening at finite temperatures is due to the anharmonic a-a interaction potential (LJ potential) and does not show up when we replace the a-a interaction with a harmonic potential. One important difference between the finite-temperature (with finite stiffness) results and the finite-size effects is that the finite-temperature effects do not generate secondary peaks while the finite-size effects do. We note that the secondary peaks (due to finite-size effects) are real physical effects, not numerical artifacts. At $T=0.1$, the energy for the KS orientation (solid squares in Fig. 2) near $\rho=1.155$ is about -0.086ϵ and lower than the minimum energy of the NW orientation (see Table II). Thus, the KS orientation is more stable than the NW orientation. In fact, we find no minimum at $\rho=1.155$, $\theta=0°$ in a finite-temperature simulation at $T=0.1$. As the stiffness of the overlayer lattice increases [i.e., the velocity of sound in Eq. (4) increases] $E^{(2)}$ decreases and size effects dominate the broadening. When the a-a interaction-potential strength increases to 16 times that of the a-s interaction, the MD results at $T=0.1$, are almost the same as the zero-temperature rigid-lattice calculation in which the NW orientation is stable near $\rho=1.155$.

In conclusion, we have developed a mapping technique to study epitaxy in lattice-mismatched partially commensurate interfaces. An application of this theory to the fcc(111)/bcc(110) interface correctly predicts the experimentally observed epitaxial orientations. A finite-temperature calculation using second-order perturbation theory and a molecular-dynamics simulation predicts a broadening of the energy minima as a function of lattice parameters. As a consequence, transitions from one epitaxial orientation to the others should be observable as a function of cluster size and stiffness of lattice.

This work is supported by NSF, Grant No. DMR 87-01921. Supercomputer time has been provided by the University of California, San Diego, Supercomputer Center.

[1]See, for example, *Epitaxial Growth,* edited by J. W. Mathews (Academic, New York, 1975); B. A. Joyce, in *Molecular Beam Epitaxy and Heterostructures,* edited by L. L. Chang and K. Ploog, NATO Advanced Study Institutes, Ser. E, Vol. 87 (Plenum, New York, 1985); J. A. Venables, Vacuum **33**, 701 (1983), and references therein.

[2]See, for instance, various articles in MRS Bull. **8** (1988).

[3]For a comprehensive list of epitaxial systems, see E. Grünbaum, in *Epitaxial Growth* (Ref. 1), p. 611.

[4]A. Kobayashi and S. Das Sarma, Phys. Rev. B **35**, 8042 (1987); R. Ramirez, A. Rahman, and I. K. Schuller, Phys. Rev. B **30**, 6208 (1984); L. A. Bruce and H. Jaeger, Philos. Mag. A **38**, 223 (1978).

[5]J. H. van der Merwe and M. W. H. Braun, Appl. Surf. Sci. **22/23**, 545 (1985); J. H. van der Merwe, Philos. Mag. A **45**, 127 (1978); **45**, 145 (1978); **45**, 159 (1978).

[6]J. A. Venables, G. D. T. Spiller, and M. Hanbucken, Rep. Prog. Phys. **7**, 399 (1984); J. D. Weeks and G. H. Gilmer, Adv. Chem. Phys. **40**, 157 (1979); D. Kashchiev, J. Cryst. Growth **40**, 29 (1977).

[7]A. Madhukar and S. V. Graisas, CRC Crit. Rev. Solid State Mater. Sci. **14**, 1 (1988); A. Kobayashi and S. Das Sarma, Phys. Rev. B **37**, 1039 (1988), and references therein.

[8]S. M. Paik and S. Das Sarma, Phys. Rev. B **39**, 1224 (1989); M. Schneider, A. Rahman, and I. K. Schuller, Phys. Rev. Lett. **55**, 604 (1985); Phys. Rev. B **36**, 1340 (1987); for a review, see I. K. Schuller, MRS Bull. **8**, 23 (1988).

[9]H. Homma, K. Y. Yang, and I. K. Schuller, Phys. Rev. B **36**, 9435 (1987).

[10]$\rho=b_a/b_s$ is a rational number for 1D interfaces. On a 2D interface, the ratio of the projection of the lattice-constant vectors on commensurate axes will be rational numbers.

[11]The surface-lattice-constant vectors for bcc(111) and fcc(110) are $\mathbf{A}=b_s(1,\sqrt{2})/\sqrt{3}$ and $\mathbf{B}=b_a(1,\sqrt{3})/2$. For two lattices to be commensurate, the ratio of both x (B_x/A_x) and y components (B_y/A_y) of the lattice-constant vectors should be rational numbers. However, in this system, the x and y components cannot be rational numbers simultaneously for any lattice-constant ratio and relative orientation.

[12]G. Kurdjumov and G. Sachs, Z. Phys. **64**, 325 (1930).

[13]G. Wassermann, Arch. Eisenhuettenwes. **126**, 647 (1933); Z. Nishiyama, Sci. Rep. Tohoku Univ. **23**, 638 (1934).

[14]Classification as first- and second-order axial commensuration is due to the leading-order contribution term in the Fourier series of the a-s interaction.

[15]S. M. Paik and I. K. Schuller (to be published).

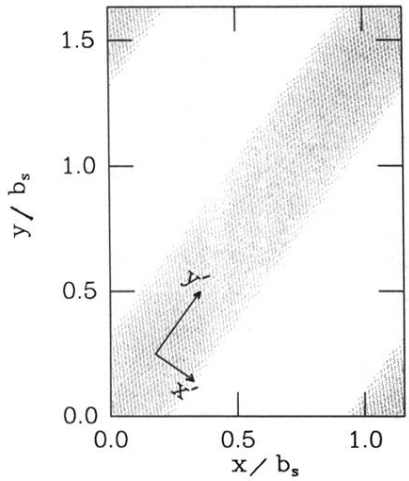

FIG. 1. The mapping pattern, $f(\mathbf{r})$, for a 9961 circular adatom cluster near KS orientation. x' and y' denote commensurate and incommensurate axes, respectively.